Effect of Numerical Dispersion in FDTD Simulations of Light Scattering from Photoreceptors

Samer S. Abdallah[1], Alexandre Iolov[2,1], Kostadinka Bizheva[2] and Omar M. Ramahi[1,2]

[1] Department of Electrical and Computer Engineering
[2] Department of Physics and Astronomy
University of Waterloo
Waterloo, ON, N2L3G1, Canada
oramahi@ece.uwaterloo.ca

Abstract ─ Recently, the FDTD method was used to investigate the optical functional response of retinal photoreceptors. Light scattering patterns of the cells were simulated under various hypothetical states to determine the physiological processes that are most likely responsible for the experimentally observed signals. An FDTD model of a photoreceptor cell spans several wavelengths, therefore, the numerical dispersion, inherent in FDTD algorithms, will introduce significant phase errors in the simulation results. These phase errors can lead to erroneous predictions, especially for narrow band light stimulus. Currently, the qualitative and quantive effects of numerical dispersion on light scattering computations are still unknown. In this paper, an analysis of the numerical dispersion errors in the near and far scattered fields is performed. The analysis provides decision guidelines for selecting enough computational resources to obtain the light scattering patterns with acceptable margin of errors.

Index Terms ─ Finite-difference time-domain, biomedical applications, scattering, numerical simulation, time-domain analysis.

I. INTRODUCTION

A large number of diseases can cause various changes in the structural and physiological properties of biological tissues. Previous research studies [1-2] have shown that such changes can affect light scattering patterns of the infected cells.

Therefore, the interest in numerical simulations of light scattering from biological tissue has increased significantly in the past years [3-5], especially with the advent of parallel processing and the increase in available computational resources. In most cases, the finite-difference time-domain (FDTD) method was the preferred numerical technique due to its simplicity in modeling large and complex structures such as the biological cells. Recently, we have used the FDTD method in investigating the causes of the optical functional response of retinal photoreceptors cells [6, 7]. The goal was to understand which of the physiological processes that can affect the power of the backscattered light.

When compared to the exact analytical solution, the FDTD results suffer from phase errors that originate from the discrete nature of the FDTD algorithms. For second-order accurate finite-difference algoirthms, the phase errors strongly depend on the ratio of wavelength to the grid meshing size [8]. Therefore, the effect of the errors on a propagating signal is similar to the effect of propagation in a dispersive material, and consequently, the term ``numerical dispersion'' was coined for this class of errors. In general, reducing the effect of numerical dispersion is constrained by the computational resources and the size of the problem since halving the phase errors requires the doubling of the resolution (i.e., doubling the mesh size in all directions). The main trade-off is between computational resources and accuracy. Moreover, numerical dispersion is more severe in electrically large structures which spans

several wavelengths since the error in phase can accumulate up to a $180°$ phase reversal during the propagation in the space-time coordinate system. Currently, there are no studies that quantify the error introduced by the numerical dispersion in the scattering profiles. Therefore, the meshing step is usually set to the minimum possible value. This approach consumes large computational resources in terms of memory, processing units, storage and it will increase the waiting time for simple profiling first round simulations.

In this paper, in light of the increasing interest in the use of the FDTD method to simulate wave interaction with biological media, we study the critical effect of numerical dispersion in light scattering simulations. The nature and magnitude of errors introduced in the scattering profiles for a given mesh size are investigated while making a distinction between results calculated for the near field vs. those calculated for the far field. While the focus here is related to our work on light scattering from retinal photoreceptors, the results obtained have direct implication to the general problem of scattering from electrically-long biological tissues. The results and conclusions reached here will help to optimize computational resources when applying FDTD for scattering related problems.

II. PHYSICAL VS. NUMERICAL DISPERSION

Numerical dispersion is manifested by the modification of the real wavenumber k to a numerical wavenumber $\widetilde{k}$. Eq. 1 shows how the wave dispersion equation in FDTD depends on the time step Δt and the mesh step Δz [8]. The stability of the FDTD algorithm constrains the Courant factor $C = v\Delta t/\Delta z$ to be less than $1/dim^{1/2}$ (less than $1/3^{1/2}$ for 3D simulations). Setting the Courant factor to 0.5, $\widetilde{k}$ can be simply expressed as a function of the relative mesh size $\Delta z/\lambda$ (eq. 2) and the solution will be stable up to the coarse meshing of $\lambda/\Delta z = 10$. In the case of sinusoidal waves, the numerical phase velocity can be calculated using eq. 3 [8]. Figure 1 presents a plot of the ratio of the numerical phase velocity to theoretical one versus the relative mesh size. The maximum phase error introduced in a structure spanning m number of wavelengths can be

calculated using eq. 4 [8]. Fig. 2 shows the phase error introduced in a sinusoidal wave after propagating a distance of 10λ (i.e. $m=10$). From these results we observe that for a structure of several wavelengths, a small change in the relative mesh size can lead to a phase error of several degrees (see Fig. 2).

$$\widetilde{k} = \frac{1}{\Delta Z}\arccos\left\{1 + (\frac{\Delta Z}{c\Delta t})^2[\cos(\omega\Delta t)-1]\right\} \quad (1)$$

$$\widetilde{k} = \frac{1}{\Delta Z}\mathbf{arccos}\left\{1 + 4[\mathbf{cos}(2\frac{\Delta Z}{\lambda})-1]\right\} \quad (2)$$

$$\widetilde{v}_p = \frac{\omega}{\widetilde{k}} = \frac{2\pi f}{\frac{1}{\Delta Z}\arccos\left\{1 + 4[\cos(2\frac{\Delta Z}{\lambda})-1]\right\}}$$

$$= \left\{\frac{\frac{\Delta Z}{\lambda}}{\arccos\left\{1 + 4[\cos(2\frac{\Delta Z}{\lambda})-1]\right\}}\right\}v_p \quad (3)$$

$$\Delta\phi = m\lambda\frac{\Delta Z}{\lambda}\left(1 - \frac{\widetilde{v}_p}{v_p}\right)\times 360°. \quad (4)$$

In an ideal world where computational resources are infinite, one would like to have the lowest relative mesh size ratio as it yields the lowest phase error. The FDTD method, while extremely robust, flexible and having the ability to model a wide range of problems, demands excessive computational resources. In the coming sections, we show that optimal simulation does not necessarily imply lower relative mesh size. The reason is that not only the computational efficiency of the simulation has to be taken into account but also the target of the simulation (viz., fixed field point, distributed field, near-field monitor point vs. far-field monitor point, etc.).

III. NUMERICAL METHODS

A. Overview

In light scattering computations using the FDTD method, there are two processing steps: The first step consists of the FDTD solution of the interaction of an incident wave with a scattering object. At the end of the first step, the near-fields over a surface enclosing the object are stored. The second step consists of the near-to-far field transformation which integrates the contribution of all near-fields at the far zone. Numerical

dispersion is introduced in the first step and it has been suggested in [9] that the integration aspect of the near-to-far field transform can mitigate the phase errors, therefore, reducing the weight of the numerical dispersion on the scattering profiles. In investigating the effect of numerical dispersion on light scattering, separate analyses were made for the near- and far-fields results.
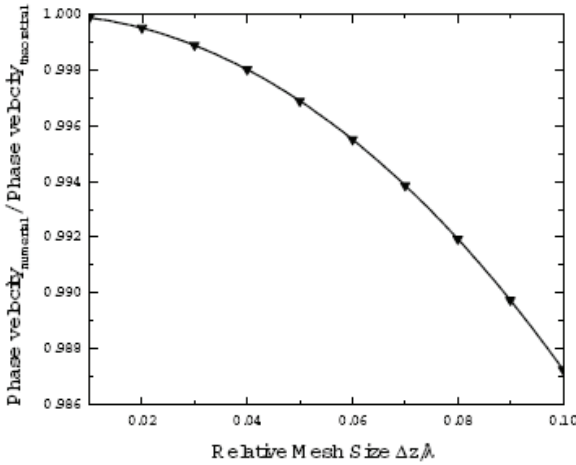

Fig. 1. Relative numerical phase velocity vs. relative mesh size. The numerical phase velocity is taken relative to the theoretical one.
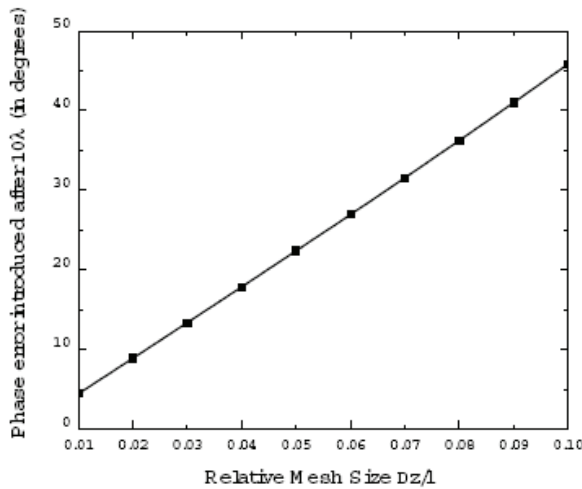
Fig. 2. Numerical phase error (in degrees) vs. relative mesh size. The error is introduced in the phase of a sinusoidal signal which propagated a distance of 10λ.

B. Model

Since we are interested in quantifying the errors in the simulations of light scattering patterns of the photoreceptors, the scattering object was selected to match the basic photoreceptor model, shown by the solid cylinder in fig. 3. The refractive index for the host medium is $n_0=1.34$ and for the cylinder is $n_1=1.41$. The effect of numerical dispersion on the model was simulated by increasing progressively the mesh size in the axial direction since the incident wave travels for the longest distance and duration in this direction. The incident plane wave pulse has 100nm bandwidth around a central wavelength of $\lambda_{cen} = 1\mu m$. The simulations were performed for three cylinders of different diameters (0.1μm, 1μm and 5μm. These different apertures are meant to be representative of the three distinct scattering regimes: In the first regime, λ, the wavelength of the excitation is greater than $\sigma^{1/2}$ where $\sigma = \pi d^2/4$ is the scattering cross section area and d the diameter of the cylinder. In the second regime, λ is comparable to $\sigma^{1/2}$ and in the third regime, λ is smaller than $\sigma^{1/2}$.

C. Near-Fields Analysis Method

The analysis of the near-fields consists of determining the error in phase introduced during the propagation of the plane wave from its insertion point at the Total-Field Scattered-Field (TF-SF) boundary to the opposite boundary, going through the solid cylinder representing the photorecyptor. Two time-domain point monitors were positioned along the main axis of the cylinder to record the time signals that will be used in the processing (see Fig. 3). The first time-monitor records the incident plane wave entering the TF region whereas the second time-monitor records the signals reaching the other end of the TF region. The incident signal recorded by the first time-domain monitor was used to create the propagated incident signal as it should be theoretically at the location of the second time-domain monitor.

Figure 4 presents the processing flow used to implement the ideal propagation of the incident signal. A Discrete-Fourier-Transform (DFT) transforms the incident pulse into the frequency
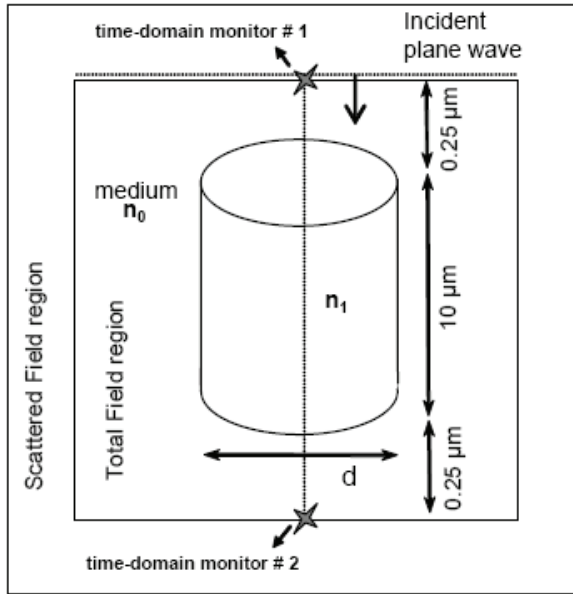
Fig. 3. The setup of the FDTD simulations for numerical dispersion. The stars show the locations of the time-domain monitors used. The refractive index for the host medium is $n_0=1.34$ and for the cylinder is $n_1=1.41$.

domain, then each frequency component is selected and inverse transformed back to the time-domain using Inverse-Discrete-Fourier-Transform (IDFT). The harmonical signal obtained in the previous step is multiplied by the phase factor e^{-kx} where k is the wavenumber corresponding to the frequency f and to the medium of propagation with length ΔL and refractive index n (c is light celerity). Finally, all time sub-signals are integrated to generate the ideally propagated signal $S_{theoretical}$. Ideally, $S_{theoretical}$ has zero phase error and therefore, the difference in phase when compared to the FDTD signals recorded by the second time-domain monitor approximates the phase error introduced by the numerical dispersion. It is important to note that the wave number k used in the phase translation e^{-kx} takes into account the different media encountered along the path of propagation (*viz.*, the media n_0 and n_1, see Fig. 3.)

Figure 5 presents the processing diagram for the computation of phase errors in the near fields point signals. First, the DFT signals of both reference (i.e. theoretical) and target (i.e. simulated) signals were computed to determine the spectrum of interest. Then each frequency

component is selected and inverse transformed back to the time-domain using IDFT. The time-domain sub-signals are inputted to the hilbert analyzer which computes the phase difference. The phase difference are reported per each frequency of the source signal spectrum.
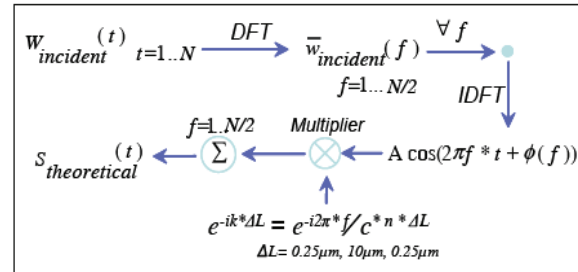

Fig. 4. Processing flow showing the generation of the theoretical signal $S_{theoretical}$ with ideally zero phase error. $S_{theoretical}$ was obtained from an ideal propagation of the incident signal recorded by the first time-domain monitor toward the location of the second time-domain monitor.
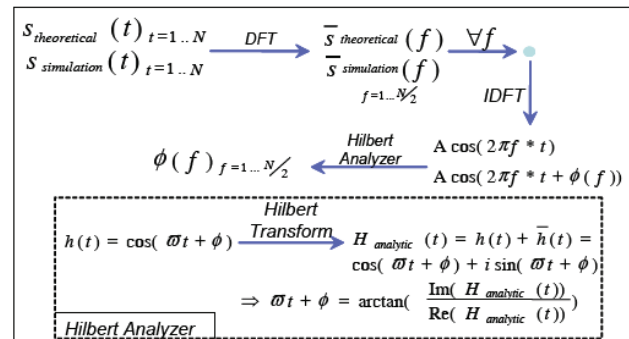

Fig. 5. Diagram of processing to determine numerical dispersion.

IV. NUMERICAL SIMULATION RESULTS

A. Near-Fields Results

Figure 6 shows the phase error introduced in the near-fields data after propagating through the TF region. The figure shows that, as the mesh size increases, the phase error at the smaller wavelengths starts to increase at a faster rate compared with the errors at the longer wavelengths. For relative mesh sizes $\lambda/\Delta z > 0.02$, this difference in phase error can pass the 200%. Fig. 7 presents the phase error occurring at the
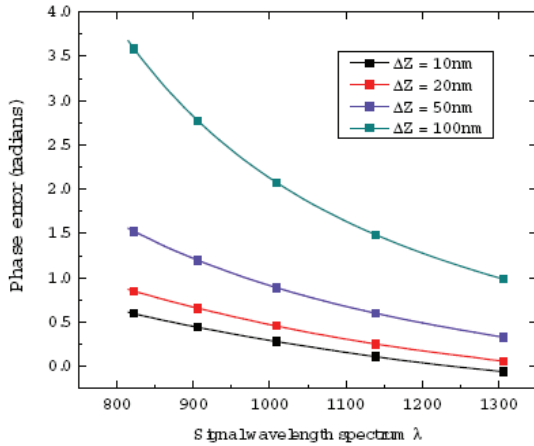
Fig. 6. Phase error plotted vs. signal wavelength spectrum for various mesh sizes ($\lambda/\Delta z$=0.01, 0.02, 0.05 and 0.1).
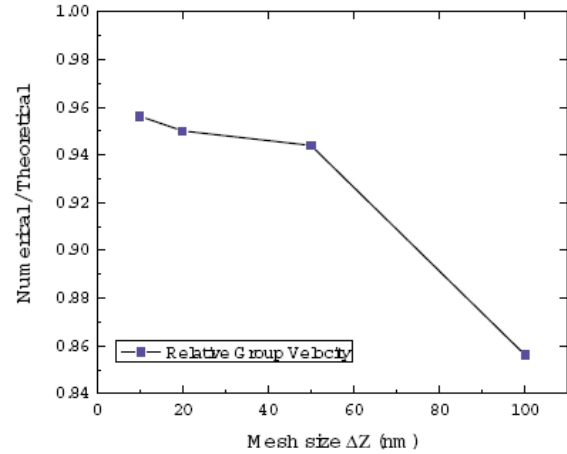

Fig. 8. Ratio of average phase velocity to the theoretical phase velocity plotted vs. mesh sizes ($\lambda/\Delta z$ =0.01, 0.02, 0.05 and 0.1).
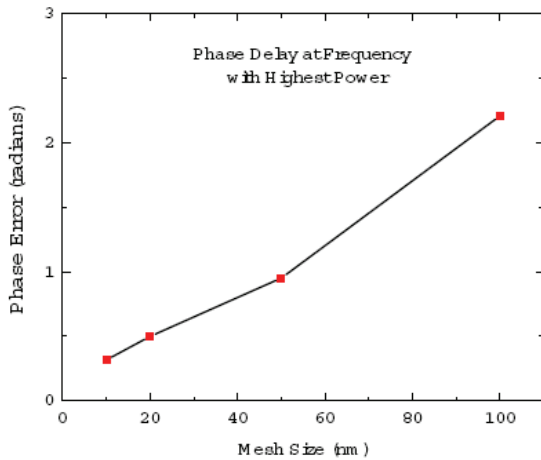

Fig. 7. Phase error at median spectrum wavelength (with highest power) plotted vs. mesh sizes ($\Delta z/\lambda$=0.01, 0.02, 0.05 and 0.1).
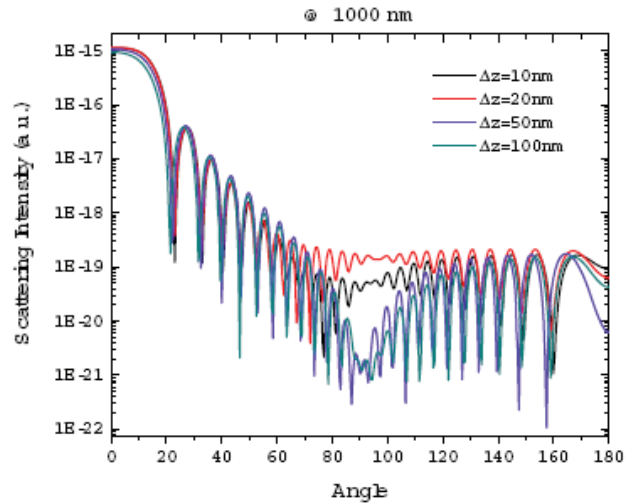

Fig. 9. Effect of numerical dispersion on light scattering in the case of small scattering cross section as compared to the wavelength (case 1).

median wavelength with peak power λ=100nm. The result compares well with the theoretical phase error calculated for the same wavelength and presented in fig. 1. Also, it shows that for a structure of 10λ, the error in phase in the near-fields is less than 180° for most practical meshing sizes and less than 90° for mesh size satisfying $\Delta z/\lambda < 0.06$.

Figure 8 presents the ratio of the average phase velocity of the propagated signal. The results show significant deviations and faster decrease as a function of the mesh size when compared with phase velocity values reported by

the theoretical analysis done in Fig. 1.

The analysis of the effect of numerical dispersion on near-fields showed that the phase error will not exceed 90° for mesh size satisfying $\lambda/\Delta z>0.05$. Also, over a spectrum of 100nm=$\lambda_{central}/10$, the variation in phase error will not exceed 60°, again for mesh sizes $\Delta z/\lambda < 0.05$. Above these thresholds, the variations show a deviation from the linear behavior where the phase error can change by values up to 180°. In terms of phase velocity, the change is less or equal to 5° for mesh size satisfying $\Delta z/\lambda < 0.05$ and can reach 15°

for mesh size satisfying $\Delta z/\lambda < 0.1$.

B. Far-Fields Results

The far-fields results consist of scattering profiles computed for each mesh size. The errors can only be reported relative to the case of finest grid since there is no analytical solution for light scattering from a finite cylinder where the incident wave propagates along the axial direction.

The far-fields results are reported for the three regimes of scattering as explained earlier. Fig. 9 shows the light scattering profile for the first regime, where the wavelengths of the signal are much greater than the diameter of the cylinder. In this case, numerical dispersion has the greater effect around the normal scattering directions where the sidelobes experience large fluctuations in their magnitude. The sidelobes in the forward and backscattering directions show a slight shift towards lower angles.
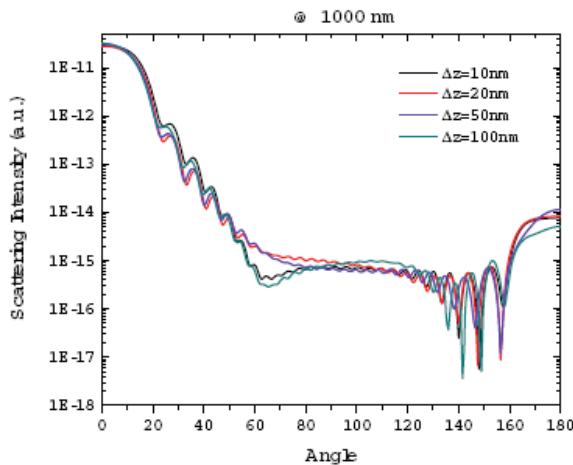

Fig. 10. Effect of numerical dispersion on light scattering in the case of medium scattering cross section as compared to the wavelength (case 2).

Fig. 10 presents the light scattering profile for the second regime of scattering where the diameter of the cylinder is comparable to the wavelengths of the signal. In this regime, the sidelobes around the normal directions start to show less magnitude fluctuations and more positional fluctuations whereas the opposite happens in the normal and backscattered directions. Fig. 11 presents the light scattering profile for the third regime of scattering where the diameter of the cylinder is larger than the wavelengths of the signal. In this regime, the

sidelobes around the normal directions show slight variations in magnitude whereas the sidelobes of the backscattered and forward regions show a mix of large magnitude and positional changes.
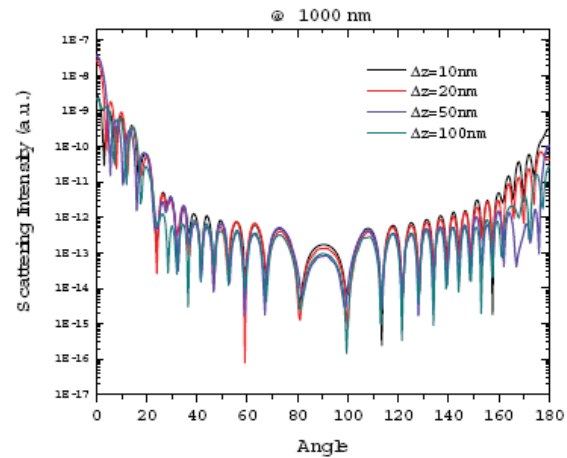

Fig. 11. Effect of numerical dispersion on light scattering in the case of large scattering cross section as compared to the wavelength (case 3).

V. CONCLUSION

We have investigated the effect of numerical dispersion on light scattering profiles obtained from simulations of retinal photoreceptors models. The near-fields results quantified the maximum phase error and the relative phase velocity observed versus the meshing size. Far-fields results show that the numerical dispersion either affects the sidelobes in forward and backscattering regions or the sidelobes in the normal scattering directions. The normal direction sidelobes are less affected as the aperture increases whereas the opposite happens for the sidelobes of the forward and backscattering regions. The results presented show that, depending on the simulation objectives, the relative mesh size ratio can be optimally selected to achieve sufficient accuracy while minimizing the computational requirements of the FDTD method.

VI. ACKNOWLEDGMENTS

REFERENCES

[1] M. J. Piket-May, A. Taflove, and J. B. Troy, "Electrodynamics of visible light interactions with the vertebrate retinal rod," *Optics Letters*, vol. 18, pp. 568-570, 1993.

[2] A. K. Dunn, *Light Scattering Properties of Cells,* Phd, Univ. Texas at Austin, 1997)

[3] A. Dunn, C. Smithpeter, A. J. Welch, and R. Richards-Kortum, "Finite-difference time-domain simulation of light scattering from single cells," *J. Biomed. Opt.*, vol. 2, no. 3, pp. 262—266, 1997.

[4] R. Drezek, A. Dunn, and R. Richards-Kortum, "A pulsed finite-difference time-domain (FDTD) method for calculating light scattering from biological cells over broad wavelength ranges", *J. Opt. Express,* vol. 6, no. 7, pp. 147-157, 2000.

[5] R. Drezek, M. Guillaud, T. Collier, I. Boiko, A. Malpica, C. Macaulay, M. Follen, and R.Richards-Kortum, "Light scattering from cervical cells throughout neoplastic progression: influence of nuclear morphology, DNA content, and chromatin texture", *J. Biomed. Opt.,* vol. 8, no. 1, pp. 7-16, 2003.

[6] S. S. Abdallah, *Finite-Difference Time-Domain Simulations of Light Scattering from Retinal Photoreceptors,* Electrical Eng., Univ. of Waterloo, 2007.

[7] S. S. Abdallah, O. M. Ramahi, and K. Bizheva, "FDTD Simulation of Electromagnetic Wave Scattering from Retina Cells", *The 29th Annual International Conference of IEEE Engineering in Medicine and Biology Society*, pp. 1639-1642, 2007.

[8] T. Taflove, and S. C. Hagness, *Computational Electrodynamics: The Finite-Difference Time-Domain Method*, 2nd ed. Norwood, MA: Artech House, 2000.

[9] F. D. Hastings, J. B. Schneider, and S. L. Broschatc, "A finite-difference time-domain solution to scattering from a rough pressure-release surface," *J. Acoust. Soc. Am.,* vol. 102, no. 6, pp. 3394-3400, 1997.